Unravelling the Reaction Mechanism of SiO Anodes for Liion Batteries by Combining in situ 7Li and ex situ 7Li/29 Si Solid-state NMR Spectroscopy

DOI:
10.1021/jacs.9b01589

Document Version
Accepted author manuscript

Unravelling the Reaction Mechanism of SiO Anodes for Li-ion Batteries by Combining *in situ* ^{7}Li and *ex situ* ^{7}Li/^{29}Si Solid-state NMR Spectroscopy

Journal:	*Journal of the American Chemical Society*
Manuscript ID	ja-2019-01589u.R1
Manuscript Type:	Article
Date Submitted by the Author:	08-Apr-2019
Complete List of Authors:	Kitada, Keitaro; Murata Manufacturing Co Ltd; University of Cambridge Department of Chemistry Pecher, Oliver; University of Cambridge, Chemistry Magusin, Pieter; University of Cambridge, Chemistry Groh, Matthias; University of Cambridge Department of Chemistry, Weatherup, Robert; University of Manchester School of Chemistry, The University of Manchester Harwell Campus Grey, Clare; University of Cambridge, Chemistry

Unravelling the Reaction Mechanism of SiO Anodes for Li-ion Batteries by Combining *in situ* ^{7}Li and *ex situ* ^{7}Li/^{29}Si Solid-state NMR Spectroscopy

Keitaro Kitada,[a,b] Oliver Pecher,[b,c] Pieter C. M. M. Magusin,[b] Matthias F. Groh,[b] Robert S. Weatherup,[b,d,e] and Clare P. Grey[b,*]

[a] Murata Manufacturing Co., Ltd., 1-10-1 Higashikotari, Nagaokakyo-shi, Kyoto 617-8555, Japan

[b] University of Cambridge, Department of Chemistry, Lensfield Road, Cambridge CB2 1EW, United Kingdom

[c] NMR Service GmbH, Blumenstr. 70 Haus 3, 99092 Erfurt, Germany

[d] School of Chemistry, University of Manchester, Oxford Road, Manchester, M13 9PL, United Kingdom

[e] University of Manchester at Harwell, Diamond Light Source, Harwell Campus, Didcot, Oxfordshire, OX11 0DE, United Kingdom

ABSTRACT

Silicon monoxide is a promising alternative anode material due to its much higher capacity than graphite, and improved cyclability over other Si anodes. An in-depth analysis of the lithium silicide (Li_xSi) phases that form during lithiation/delithiation of SiO is presented here and the results are compared with pure-Si anodes. A series of anode materials is first prepared by heating amorphous silicon monoxide (a-SiO) at different temperatures, X-ray diffraction and ^{29}Si NMR analysis revealing that they comprise small Si domains that are surrounded by amorphous SiO_2, the domain size and crystallinity growing with heat treatment. *In* and *ex situ* ^{7}Li and ^{29}Si solid-state NMR combined with detailed electrochemical analysis reveals that a characteristic metallic Li_xSi phase is formed on lithiating a-SiO with a relatively high Li concentration of x = 3.4-3.5, which is formed/decomposed through a continuous structural evolution involving amorphous phases differing in their degree of Si-Si connectivity. This structural evolution differs from that of pure-Si electrodes where the end member, crystalline $Li_{15}Si_4$, is formed/decomposed through a two-phase reaction. The reaction pathway of SiO depends, however, on the size of the ordered Si domains within the pristine material. When crystalline domains of 5 nm within a SiO_2 matrix are present, a phase resembling $Li_{15}Si_4$ forms, albeit at a higher overpotential. The continuous formation/decomposition of amorphous Li_xSi phases without the hysteresis and phase change associated with the formation of c-$Li_{15}Si_4$, along with a partially electrochemically active SiO_2/lithium silicate buffer layer, are paramount for the good cyclability of a-SiO.

INTRODUCTION

Lithium-ion batteries (LIBs) have become the essential, portable energy source for modern industrial products, due to their high-voltage and high-energy density. While the energy density of LIBs continues to increase year on year, both the miniaturization of portable electronics – necessitating smaller but higher energy density batteries - and the transition towards vehicle electrification – requiring larger, cheaper and higher energy density batteries – means that the demand for further improvement remains intense.[1] Graphite has historically been used as the anode of choice for LIBs, but its capacity is limited to 372 mAh/g.[2] To exceed this limit, silicon (Si) based materials have been proposed, which offer up to ten times larger gravimetric and volumetric capacities.[3] However, the large volume increase of Si during lithiation and thus of Si based anodes contributes to mechanical failure of the cell components.[4] The formation of crystalline $Li_{15}Si_4$ (c-$Li_{15}Si_4$), the most (electrochemically) lithiated state of Si when cycled at room temperature, is known to cause particularly significant capacity fade during repeated cycling of such composite anodes.[5] During delithiation, this phase is directly converted to an amorphous Li_xSi phase with much lower Li content, via a two-phase reaction.[4, 6] The abrupt volume change at the two-phase interface induces huge local stress, resulting in cracking of the Si particles[7], unless nano-sized Si particle is used.[8] The newly exposed surfaces are not coated with the passivating solid-electrolyte interphase (SEI) layer and thus react with electrolyte, irreversibly consuming Li ions and resulting in electrically disconnected Si nanoparticles, both contributing to capacity fade. The simplest way to avoid this issue is to restrict the electrode potential so that it does not drop below the c-$Li_{15}Si_4$ formation potential of 50 – 70 mV vs. Li/Li^+.[4, 6, 9] However, this strategy sacrifices the capacity of the electrode; and practically it is often difficult to control the anode potential accurately enough when combined with a cathode in a commercial full cell design. Moreover, this potential control method cannot be applied to the promising Si/graphite composite anodes which represent a compromise between improved capacity and electrode stability. This is because a significant fraction of graphite's overall capacity is close to the c-$Li_{15}Si_4$ formation potential.[5, 10-13]

Silicon monoxide, SiO, has been proposed as a promising LIB anode material with a much better cyclability than conventional Si anodes.[14] SiO exists as a nano-composite consisting of Si and SiO_2 domains and silicon suboxides $SiO_{x<2}$ at the interfaces between these two components.[15] The average silicon to oxygen ratio is almost one, because this material is fabricated using SiO gas, SiO being electronically related to carbon monoxide. The crystallinity of the Si domains depends critically on the preparation conditions.[16, 17] The lithiation of SiO has previously been investigated, with no crystalline phase formation reported for amorphous SiO (a-SiO) when fully lithiated, suggesting that the suppression of c-$Li_{15}Si_4$ formation contributes to the good cyclability; thus SiO may also be promising as a component in composite electrodes with graphite. Despite its promise, the chemical evolution and compounds formed during SiO lithiation remain the subject of debate, preventing a rational choice of an optimized SiO anode.[18-30] In particular, the role of the SiO_2 and/or lithium silicates and size of (any) silicon domains and the role in these structural and morphological motifs in performance remains unclear. Most reports have identified at least two phases in lithiated SiO, a lithium silicide (Li_xSi) phase and a lithium silicate (as summarized in Table S1, supporting information). However, even the Li concentration in the Li_xSi phase, and composition and electrochemical reactivity of the lithium silicate phase remain controversial, although these are very fundamentals aspect that underpin the reaction mechanism(s). This debate reflects the significant complexity of SiO lithiation and challenges in characterization of the lithiated products: (a) lithiated products are either of low crystallinity or amorphous, (b) multiple components are present, (c) the "crystal" structures are expected to depend on the electrode potential, and (d) depending on the SiO

preparation, different crystalline phases may be present whose electrochemical behavior varies.[31, 32]

Previously, we investigated the chemical structures in electrochemically lithiated pure-Si electrodes by *in situ*/*ex situ* ^{7}Li solid-state nuclear magnetic resonance (NMR) and pair distribution function (PDF) analysis.[9, 33, 34] Figure 1 illustrates the formed local Li_xSi structures, and their corresponding ^{7}Li NMR shifts. The only crystalline phase formed in the electrochemical lithiation of pure-Si is a c-$Li_{15}Si_4$-like structure (phase 3) at the end of the lithiation process. This phase appears to tolerate a degree of Li non-stoichiometry, with a range of ^{7}Li NMR chemical shifts from 8 to −13 ppm being observed, corresponding to stoichiometry changes of approximately 0.02 – 0.03 Li per 4 Si.[9] The lower frequency shifts are observed for samples formed electrochemically on lithiation; they are associated with the highest Li contents and were referred to as "overlithiated $Li_{15}Si_4$" in previous publications.[33] At lower Li concentrations, the Li_xSi phases are known to be amorphous with two characteristic structures reported: (1) a Li_xSi phase (x<2.0) with extended Si clusters consisting of polymeric Si chains and clusters (broad ^{7}Li resonance from 0 to 10 ppm). (2) a Li_ySi phase (2.0<y<3.5) with small Si clusters consisting of two (dimers) or more connected Si atoms (^{7}Li resonances at 10 to 20 ppm); as y approaches 3.5, increasingly more isolated Si anions are present (Figure 1). The broadening observed in the ^{7}Li NMR spectra for (1) is attributed to the large distribution of chemical environments corresponding to the numerous possible polymeric structures of Si, tetrahedral coordination with Si atoms representing a dominant structural motif at these Li compositions, based on PDF studies.[34] The exact chemical shift value observed for (2) reflects the Si—Si cluster size and structure. In the crystalline small-cluster phases, Li ions near the Si pentagonal rings and stars found in $Li_{12}Si_7$ (x = 1.71) resonate at 21.8, 17.1, and –16.9 ppm,[35] the local environment resonating at –16.9 ppm resulting from Li ions in between the aromatic pentagonal rings. Li ions near Si—Si dimers resonate at 16.5 ppm (in crystalline Li_7Si_3), further lithiation to form Si-Si dimers and isolated Si (in $Li_{13}Si_4$) results in a ^{7}Li shift of 11.5 ppm. Although Si pentagonal rings are unlikely to be formed electrochemically (and indeed no resonances in this frequency range have been observed experimentally at this chemical composition) as considerable rearrangement of the sublattice is required, stars result from Si-Si bond breakage of the tetrahedral units and will thus be present as structural intermediates between extended clusters and dimers.

In this work, we systematically investigate the electrochemical lithiation of SiO at various states of charge to reveal detailed insights into the lithiation/delithiation mechanism. After electrochemical analysis and X-ray diffraction (XRD) to characterize the starting material, we apply *ex situ* ^{7}Li and ^{29}Si solid-state NMR to identify crystalline as well as amorphous Li_xSi phases to gain insights into the local Li and Si environments. In addition, we use *in situ* (sometimes also referred to as *operando* to reflect data collection during battery cycling) ^{7}Li NMR spectroscopy to monitor the formation of Li_xSi phases in real time.[36, 37] We apply our analytical approach to investigate a-SiO, and a series of disproportionated SiO (d-SiO) phases, formed by heating a-SiO to 800 to 1100 °C, in LIBs. We compare our results with those obtained from a crystalline Si (c-Si) anode, so as to investigate the influence of Si domain crystallinity and size on the formation of the different Li_xSi phases.

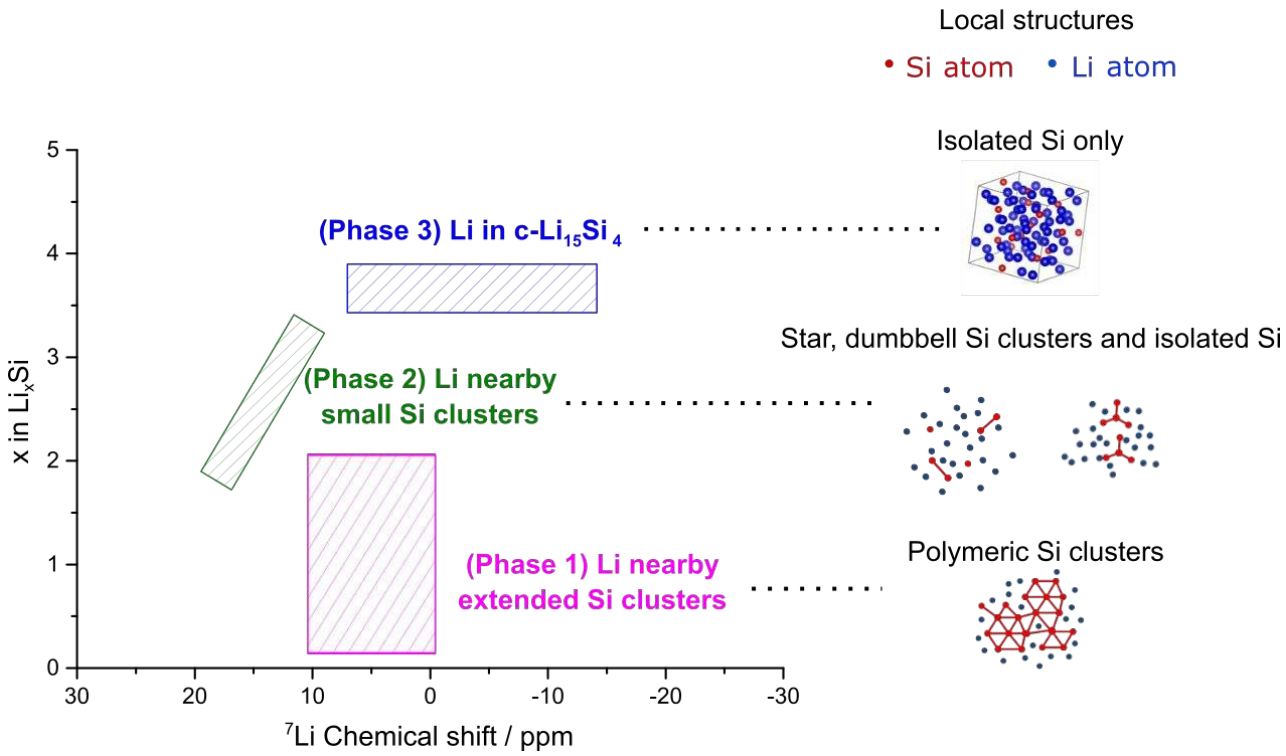

Figure 1. ^{7}Li NMR shifts and schematic structures of Li_xSi phases with different Li:Si ratios, *x*, formed by electrochemical lithiation of pure-Si and comparison with motifs found in crystalline phases at similar compositions; pink, green, and blue shaded areas represent three specific Li_xSi phases (1 – 3) containing extended Si clusters, small Si clusters, and isolated Si atoms as found in c-$Li_{15}Si_4$. Although both rings and stars are found in the crystalline phase $Li_{12}Si_7$, the former are unlikely to form electrochemically at room temperature due to the kinetic barriers associated with Si bond breakage and rearrangement. See references [9, 33, 34] for further details.

EXPERIMENTAL

Synthesis of disproportionated silicon monoxide (d-SiO)

a-SiO (OSAKA Titanium Technologies Co., Ltd., 5 μm) was packed into an Al_2O_3 crucible and heated with 5 °C/min in an electrical tube furnace under a steady Ar flow of 60 mL/min and held at 800−1100 °C for 3 h, and subsequently cooled to room temperature. The respective heat-treatment temperature for each d-SiO sample is given in parenthesis after the chemical formula in this paper, e.g. d-SiO(1000ºC) indicating heat treatment at 1000ºC.

Fabrication of electrochemical cells

Coin cells. a-SiO (OSAKA Titanium Technologies Co., Ltd., 5 μm), d-SiO (800, 900, 1000, 1050, or 1100 °C), or pure-Si (Kojundo Chemical Laboratory Co., Ltd., 99.9%, 5 μm) was mixed with carbon (Super-P, Timcal), Carboxymethyl cellulose sodium salt (CMC-Na) (Sigma-Aldrich) and deionized water in a ZrO_2 jar with two 10 mm ZrO_2 balls and was milled using a high-energy ball mill (SPEX SamplePrep's 8000M Mixer/Mill) for 40 min. Unless otherwise noted, a ratio by mass of active material : Super-P carbon : CMC-Na = 1:1:1 was used; in addition ratios of 60 : 24 : 16 and 80 : 12 : 8 were used to prepare NMR samples. The mixed slurry was coated on 15 μm copper foil on a glass plate and was dried at ambient temperature. The copper foil coated electrode was used to make coin cells for electrochemical analysis. Pellet type electrodes were used to prepare samples for *ex situ* NMR experiments. The electrodes were first coated on a glass plate, then peeled off and ground using a mortar. 50−100 mg of the ground electrode powder was pressed together onto a copper mesh at 730 MPa inside a 15 mm die set to produce a pellet electrode. All electrodes were vacuum dried at 100 °C overnight before being assembled into cells. CR2032 coin type cells were assembled with copper foil coated electrodes or pellet electrodes, using a glass fiber separator (Whatman, GLASS MICROFIBER FILTERS) and Li-metal as counter electrode and LP30 electrolyte (EC:DMC = 1:1 + 1 M $LiPF_6$). For ^{29}Si NMR samples, a polyethylene separator (Celgard® 3501) was added between the glass fiber separator and electrode to avoid glass fiber contamination of the electrode. In the case of high capacity pellet electrodes, 10 wt.-% fluoroethylene carbonate (FEC) was also added (i.e., 90:10, LP30:FEC by mass) to help avoid short circuits from Li dendrite growth at the Li metal counter electrode.

In situ cell assembly. The electrode was first coated on a glass plate, then carefully peeled off and used to prepare a free-standing film. The film was cut and pressed onto a copper mesh and glass fiber separator with a small amount of deionized water; this composite was vacuum dried at 100 °C overnight. Afterwards, it was placed into one half of a plastic cell capsule with Li-metal as the counter electrode on the other half of the cell (Figure 2). Before closing the cell, the electrolyte (EC:DMC=1:1 with 1 M $LiPF_6$ + 5 wt.-% FEC) was added.

Electrochemical measurements

Electrochemical measurements were carried out at 296(2) K using a Biologic MPG-2 battery cycler (Bio-Logic Science Instruments). Unless given otherwise, the cells were discharged to 0 mV at 1/20 C, held at 0 mV until the current reached 1/100 C, and then charged to 2 V at 1/20 C. Rest times of 10 min to 1 h were applied between the discharge and charge periods. The C-rate was calculated using an estimated specific capacity of 1900 mAh/g for the SiO samples and 3800 mAh/g for the pure-Si; additional capacity due to the Super-P/CMC-Na matrix was not considered in this calculation.

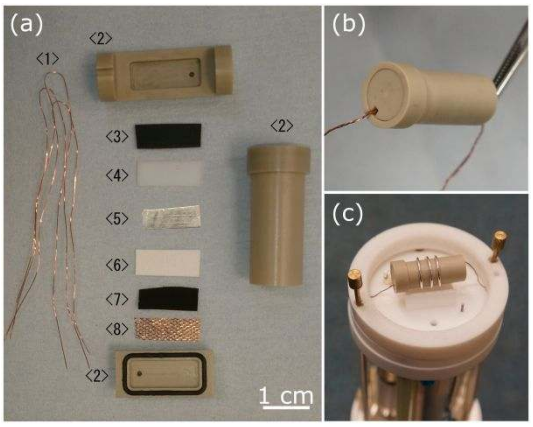

Figure 2. Assembly of the plastic cell capsule used for *in situ* NMR investigations. (a) the cell components before assembly: <1> copper wire (current collectors), <2> the three plastic (PEEK) parts of the cell with the two cavity parts on top and bottom as well as the capsule on the right, <3> Viton spacer of 1 mm thickness, <4> PTFE spacer of 0.5 mm thickness, <5> Li metal foil of 1 mm thickness, <6> glass fiber separator, <7> SiO or pure-Si / CMC-Na / Super-P free-standing electrode film, and <8> copper mesh to connect electrode and copper wire current collector; (b) an assembled plastic cell capsule with the copper wire current collectors on both sides; and (c) the plastic cell capsule set up in the coil of the Automatic Tuning Matching Cycler (ATMC) *in situ* NMR probe used for the *in situ* ^{7}Li NMR experiments.[36, 37]

Powder XRD

Powder XRD patterns of a-SiO, d-SiO, and Li_4SiO_4 were acquired at 296(2) K on a Panalytical Empyrean diffractometer equipped with a Ni filter using Cu-K_α radiation (λ = 154.06 pm, 154.43 pm) in a Bragg–Brentano setup. Rietveld refinement was performed using the TOPAS Academic software package (version 4.1).[38] The crystallite size of silicon was estimated by a Voigt-convolution approach according to Balzar *et al.*[39], assuming a lognormal size distribution. The diffuse scattering features around 20 to 25° and ~50° have each been modelled by adding an artificial peak that was independently fit in the refinement. A synopsis of the refinement parameters can be found in Table S5 (Supporting Information).

Solid-state NMR spectroscopy

Ex situ ^{7}Li and ^{29}Si NMR. Magic angle spinning (MAS) ^{7}Li NMR spectra were measured on a Bruker Avance III 500 spectrometer operating at a ^{7}Li NMR frequency of 194.35 MHz and equipped with a 4 mm MAS probe. Single-pulse excitation was used in combination with a recycle delay of 3 s. The sample rotation rate was 12.5 kHz. MAS ^{29}Si NMR spectra were recorded on Bruker Avance III 500 and Avance I 400 spectrometers operating at ^{29}Si NMR frequencies of 99.36 and 79.49 MHz, respectively. Rotor-synchronized Hahn-echo spectra were typically obtained at spinning speeds of 8 kHz with recycle delays of 1 or 30 s to detect the signals of Li_xSi or Li_4SiO_4 respectively. NMR raw data handling and processing was done using Bruker Topspin. The ^{7}Li and ^{29}Si chemical shifts were referenced to solid Li_2CO_3 and Trimethylsilylpropanoic acid both at 0 ppm, respectively.

In situ ^{7}Li NMR. In situ ^{7}Li NMR of electrochemical pouch cells was conducted on a Bruker Avance I 300 spectrometer operating at a ^{7}Li NMR frequency of 116.64 MHz using repeated single pulse excitation with a recycle delay of 0.2 s. A short recycle delay was adopted to suppress the strong signal associated with Li ions in the electrolyte. 2048 FIDs were collected for about 8 min for each spectrum and this cycle was repeated during the electrochemical measurements. The ^{7}Li chemical shifts were externally referenced to solid Li_2CO_3 at 0 ppm. The NMR raw data was processed by Bruker Topspin with manual phase correction

and automatic base line correction using a 5th order polynomial function. In parallel to the repeated recording of NMR spectra, electrochemical measurements were carried out using a battery tester (Biologic VSP, Bio-Logic Science Instruments). Unless otherwise noted, the cell was discharged in constant current–constant voltage (CC-CV) mode at 1/20 C and held at 0 mV until the current reached 1/100 C. Subsequently, after a 1 h rest period, the cell was charged to 2.0 V in CC mode. After another 1 h rest period, the cycle was repeated.

NMR data analysis. Deconvolution of ^{7}Li NMR spectrum from *in situ* and *ex situ* measurements was carried out by using the DMFIT software.[40] The NMR signal of lithium in the Super-P/CMC-Na matrix and low-lithium Li_xSi phase with extended Si cluster peaks were fitted using Lorentzian line shapes, whereas the signals of Li in the phase with small Si clusters and the m-Li_xSi phase (see below for discussion of signal assignments) were fitted by superimposed Gaussian and Lorentzian lineshapes with the same center positions but different widths, as these peaks featured sharp center as well as broad skirt components.

RESULTS

Prior to detailed NMR characterization, we first investigated the nanostructures of the a-SiO and d-SiO materials by powder XRD and their overall electrochemical lithiation properties by the use of galvanostatic measurements.

Crystallinity of a-SiO and d-SiO

The powder XRD pattern of a-SiO contains no sharp Bragg reflections and only diffuse scattering from the amorphous components are visible (Figure 3). On raising the temperature of the a-SiO heat-treatment to 900 °C, Bragg reflections due to elemental Si emerge. These grow in intensity and sharpen on raising the dwell temperature of the heat-treatment, indicating increased disproportionation of SiO and growing crystallite diameters (Figure 3). The average crystallite diameter of the silicon domains, obtained as part of a Rietveld refinement (Table S5 and Figures S11 to S14, Supporting Information) and assuming a log-normal size distribution,[39] increases from $d_{\log,900}$ = 2.2(3) nm for d-SiO(900 °C) to $d_{\log,1100}$ = 5.0(2) nm for d-SiO(1100 °C). Simultaneously, the diffuse scattering pattern from a-SiO is affected: The shift of the broad feature at 20 to 25°, 2θ, towards lower scattering angles (Figure 3, dotted line arrow) with temperature can be attributed to structural changes of the amorphous SiO_2 component, as the position of this diffuse scattering feature following heat treatment at 1100 °C resembles the scattering features of typical (boro-)silicate lab glass. In addition, the broad diffuse scattering feature around 50°, 2θ, (corresponding to "lattice" spacings of d ~180 pm; Figure 3, bracket) vanishes upon development of the Si reflections above 900 °C, thus we attribute it to short-range order in a-SiO (cf. d(Si-O) = 162 pm in α-SiO_2[41]; d(Si–Si) = 235 pm in silicon[42]).

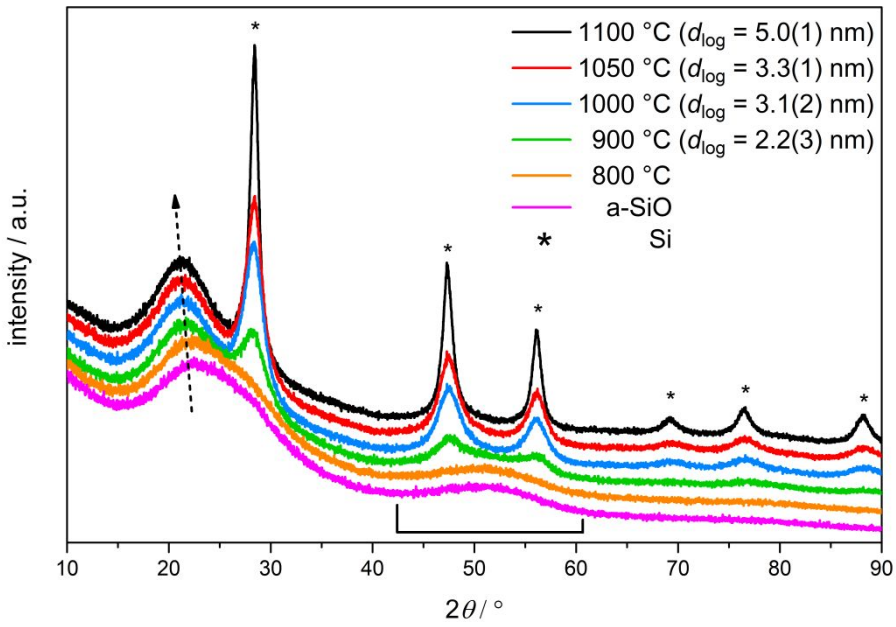

Figure 3. XRD patterns of a-SiO and heat-treated d-SiO samples. Diffraction peaks due to crystalline Si are marked with an asterisk. Average crystallite diameters (in parentheses) of the Si domains have been estimated by a Voigt-convolution approach as part of a Rietveld refinement (Figures S11 to S14, Supporting Information). Note the shift of the broad feature at a diffraction angle of 20 to 25°, 2θ, (arrow) and the disappearance of another diffuse scattering feature around 50°, 2θ, (bracket) upon treatment at higher temperatures. All samples were measured on glass-slides, which present a broad background when no sample is present, very similar to the feature at 20 to 25°, 2θ, seen for d-SiO(1100 °C) (Figure S15, Supporting Information). However, the systematic changes in XRD pattern with dwell-temperature indicates that this background does not contribute, presumably due to the rather high absorption of our samples.

Electrochemical lithiation properties

Electrochemical lithiation properties of a-SiO, d-SiO and pure-Si electrodes were investigated against Li metal using CR2032 coin type cells. Figure 4 shows the voltage-capacity profile and dQ/dV-voltage profile and Table 1 gives discharge/charge capacities and coulombic efficiencies for the initial two cycles.

Crystalline Si: The electrochemistry of the pure-Si electrode comprising 5 μm sized particles is characterized by two long pseudo-plateaus observed at 80 mV for the initial lithiation and at 420 mV in the subsequent delithiation (Figure 4a,b). The former plateau derives from the irreversible dissociation of the crystalline Si structure, whereas the latter plateau corresponds to conversion of the c-$Li_{15}Si_4$-like structure to form a-Li_xSi.[4, 9] The presence of these clear voltage processes indicates that these reactions essentially proceed via two-phase reactions. In the second and subsequent cycles, two pseudo plateaus are apparent at 250 mV and 100 mV during lithiation. They represent the formation of the extended Si cluster (phase 1) and small Si cluster (phase 2) phases, respectively (Figure 1). The more sloping nature of these processes indicates that the reactions proceed via a more gradual evolution of local structures (which could be viewed as solid solutions) rather than via two-phase reactions. A small plateau is observed at 40 mV in the initial lithiation and at 70 mV in the second cycle during lithiation (Figure 4c), which is attributable to the transformation of a-Li_xSi phase 2 to c-$Li_{15}Si_4$.[4, 9] A second cell constructed from the same electrode was then cycled with the discharge voltage restricted to 100 mV, following an initial cycle involving a discharge to 0 V to break up all of the crystalline Si (Figure 4a,b) and form amorphous Si (a-Si) on delithiation. A 420 mV plateau in the delithiation process is not observed in this case, but instead, two pseudo plateaus at 300 mV and 450 mV are apparent. These processes are assigned to the delithiation of the small Si cluster (2) and extended Si cluster phases (1), respectively, the reactions now proceeding via solid solution reactions rather than the two-phase decomposition observed for the delithiation of the c-$Li_{15}Si_4$-like structure.

a-SiO: The electrochemistry of the a-SiO electrode exhibits distinct processes at 250 and 100 mV during lithiation and at 300 and 450 mV during delithiation (Figure 4a,b). These processes are similar to those seen for pure-Si after the first "conditioning" cycle to form a-Si, and when the discharge voltage is restricted to 100 mV, i.e., when a-Si is cycled electrochemically, suggesting similar Li_xSi reactions occur. Additionally, a process at around 600 to 400 mV is observed only during the initial lithiation, which is associated with an irreversible reaction.

d-SiO: The electrochemistry of the various d-SiO electrodes varies noticeably from that of a-SiO, greater differences being observed for higher heat-treatment temperatures (Figure 4a,b). The 1st irreversible 600 to 400 mV process seen for a-SiO shifts to lower voltage with heat treatment temperature merging with the 250 mV process: following heat treatment at 800 °C it is seen as a higher voltage shoulder to the 250 mV process and it is no longer observed for d-SiO(900 °C). Although the 250 mV process is seen for d-SiO(800 °C), it also shifts to lower potential with sample treatment temperature, merging with the 100 mV process for d-SiO(1000 °C). While a single process at approximately 100 mV is observed for both d-SiO(1000 °C) and d-SiO(1050 °C), the two characteristic processes at 300 mV and 450 mV due to the delithiation of phases 2 and 1 are still observed. Almost all the lithiation during the initial discharge occurs during the 0 mV hold for d-SiO(1100 °C) on discharging at a rate of C/20 and now the processes seen on delithiation are very different: a plateau is seen at 420 mV along with a sharp peak in the dQ/dV plot, the latter suggesting that a c-$Li_{15}Si_4$-like structure is at least partially formed. The anomalously low lithiation potential observed in the d-SiO(1100 °C) initial cycle is reproducible, and was also observed in a previous d-SiO study.[19] This large over-potential is ascribed to the slow kinetics associated with (i) dissociating the

crystalline Si, (ii) lithiating the insulating (electrochemically almost inert) SiO_2 phase, and (iii) the extremely sluggish electronic and ionic transport through the SiO_2 buffer layers (as discussed below), a process required to lithiate the crystalline silicon. The processes observed in subsequent cycles are very similar to those seen for a-SiO for all the d-SiO electrodes, except for d-SiO(1100 °C). While the 250 and 100 mV processes are still observed on lithiation for SiO(1100 °C), a small plateau, which is attributed to c-$Li_{15}Si_4$-like structure formation, is observed at 40 mV on the 2nd lithiation (Figure 4c) and both a broad and sharp peak are seen in the dQ/dV plots on delithiation at 400 and 450 mV, respectively. Notably, the pure-Si and d-SiO(1100 °C) electrodes, which both exhibit a plateau associated with a c-$Li_{15}Si_4$-like structure during delithiation, have slightly lower second cycle coulombic efficiencies than the other electrodes where this feature is absent (Table 1).

Table 1. Electrochemical parameters extracted for the a-SiO, d-SiO and pure-Si electrodes shown in Figure 4. Efficiency refers to coulombic efficiency calculated from the difference between the discharge and charge capacities. All cells were cycled using constant-current/constant-voltage discharge at 0.05 C to 0 mV, constant-current charge at 0.05 C to 2.0 V except the pure-Si(100 mV) cell. The pure-Si(100 mV) cell was cycled under the same conditions as the other cells during the initial cycle (i.e., to 0 mV), and then the discharge voltage was set to 100 mV from the second cycle onwards.

Sample	Initial cycle			Second cycle		
	Discharge (mAh/g)	Charge (mAh/g)	Efficiency (%)	Discharge (mAh/g)	Charge (mAh/g)	Efficiency (%)
a-SiO	2934	1908	65.0	1943	1842	94.8
d-SiO(800 °C)	2909	1873	64.4	1922	1759	91.6
d-SiO(900 °C)	2965	1916	64.6	1981	1797	90.7
d-SiO(1000 °C)	2921	1874	64.2	1950	1761	90.3
d-SiO(1050 °C)	2877	1898	66.0	1996	1845	92.4
d-SiO(1100 °C)	2911	1627	55.9	1553	1378	88.8
Pure-Si	4212	2748	65.2	2139	1741	81.4
Pure-Si (100 mV)	4297	2806	65.3	1598	1455	91.1

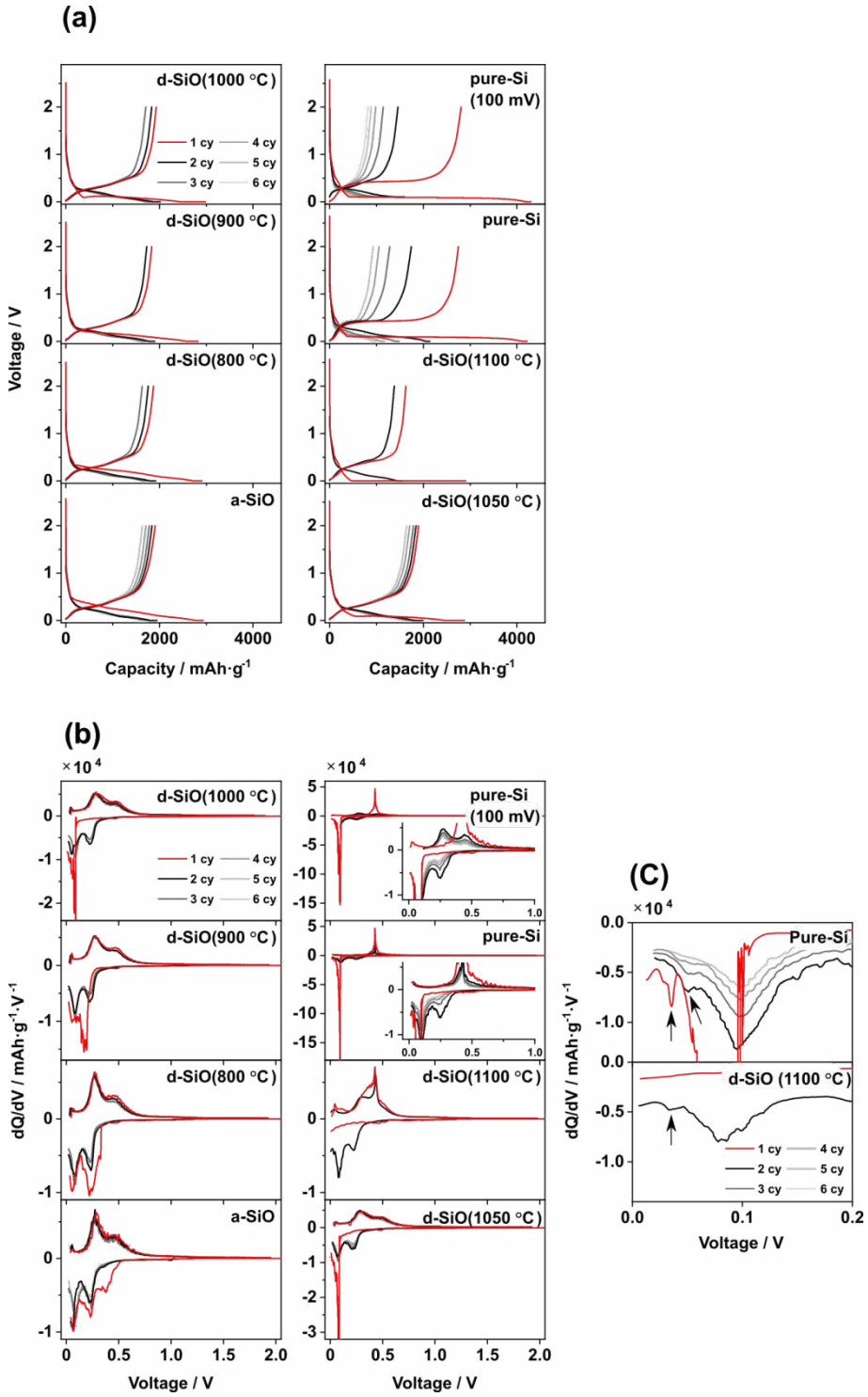

Figure 4. (a) Voltage—capacity and (b) dQ/dV—voltage profiles of a-SiO, d-SiO, and pure-Si anodes. (c) Zoom of the dQ/dV – voltage profiles of d-SiO(1100ºC) and pure-Si. The respective heat-treatment temperature of SiO is given in parenthesis after the chemical formula. Red lines represent the initial lithiation/delithiation cycle, while black and grey lines indicate subsequent cycles. All cells were cycled in constant-current/constant-voltage discharge at 0.05 C to 0 mV, constant-current charge at 0.05 C to 2.0 V except pure-Si(100 mV). The pure-Si(100 mV) cell was cycled under the same conditions as the other cells during the initial cycle, and then the discharge voltage was set to 100 mV from the second cycle onwards. Arrows in (c) show the small plateau associated with c-$Li_{15}Si_4$-like structure formation.

In situ ^{7}Li NMR

In situ ^{7}Li NMR experiments were conducted on pure-Si, a-SiO, d-SiO(1000 °C) and d-SiO(1100 °C) electrodes (Figure 5). These samples were chosen for a detailed NMR investigation, because a-SiO and d-SiO(1100 °C) represent the extremes in terms different crystallinity and electrochemical performance, while d-SiO(1000 °C) has intermediate characteristics, with electrochemistry similar to that of a-SiO but with small crystalline Si domains as in d-SiO(1100 °C). All spectra show strong signal near 0 ppm, which is from electrolyte and SEI, as well as signals in the typical Li_xSi shift region.[9, 33] The Li_xSi signal overlaps with the strong electrolyte peak as well as a peak (*ii*-label in Figure 5) that shifts with state of charge, which is related to the Super-P/CMC-Na matrix. *In situ* NMR spectra obtained for the Super-P/CMC-Na matrix alone show a weak peak at 10 ppm on discharging to 100 mV, which shifts to approximately 25 ppm as the voltage approaches 0 mV (Figures S8 and S9, Supporting Information). Deconvolution is required to distinguish the Li_xSi signals of interest from the "Super-P/SEI" peaks.

The ^{7}Li NMR spectra of pure-Si are similar to that observed previously [9, 33] and are characterized by asymmetric lithiation/delithiation behavior. During initial lithiation, a ^{7}Li NMR signal first appears at 12 ppm assigned to Li ions near small Si clusters and isolated Si (Figure 5a, *(v)*-label) which grows with time until another peak emerges at −13 ppm assigned to overlithiathed c-$Li_{15}Si_4$ (Figure 5a, *(vi)*-label) whose intensity grows whilst the 12 ppm peak shrinks. The fixed chemical shift of these peaks during lithiation suggests that in each case a constant chemical environment is maintained, indicating a two-phase reaction process: the first corresponding to the formation of an amorphous Li_xSi phase by dissociation of crystalline Si, and the second to the conversion of this phase to c-$Li_{15}Si_4$. During the first delithiation the "overlithiated" c-$Li_{15}Si_4$ resonance disappears almost immediately and no clear Li_xSi signal was observed except a broad peak (Figure 5a, *(i)*-label) near the end of delithiation, which is attributed to the lithium-poor Li_xSi phase with extended Si clusters.[9] During the second lithiation, a peak near 20 ppm due to Li ions near small Si clusters (Figure 1, phase 2) and a peak at -13 ppm (Figure 5a, *(vi)*-label) due to c-$Li_{15}Si_4$-like structures are observed (Figure 1, phase 3). The continuous shift of the peak from phase 2 suggests that the chemical composition continuously changes depending on voltage, consistent with the gradual structural transformation/solid solution-type process proposed earlier. The c-$Li_{15}Si_4$-like structure peak appears abruptly along with the disappearance of the small Si cluster peak. During the second delithiation only a broad peak attributed to Li ions in the extended Si cluster phase is observed near the end of the charge, similar to that seen during the initial delithiation. For the third lithiation, the voltage was restricted to 100 mV, which is higher than that required for c-$Li_{15}Si_4$ phase formation voltage.[4, 6, 9] In this case, no c-$Li_{15}Si_4$ peak is observed at the end of lithiation and the observed small Si cluster phase 2 peak instead continuously moves from 10 back to 20 ppm during delithiation, indicating the gradual formation of a higher concentration of Si dimers, before disappearing at the end of the low voltage process as these condense to form the large Si connected network.

In contrast to the pure-Si electrode, the a-SiO ^{7}Li NMR spectra were characterized by a much more symmetric lithiation/delithiation behavior for all cycles (Figure 5b), with almost the same evolution of ^{7}Li chemical shift repeated between lithiation/delithiation from the first to third cycle. The observed chemical shifts are 0 to10 ppm for the processes at 250 mV during lithiation and 450 mV during delithiation (Figure 5b, *(i)*-label; Figure 1, phase 1), and 8 to 15 ppm for the processes at 100 mV during lithiation and 300 mV during delithiation (Figure 5b, *(iii)*-label, Figure 1, phase 2), using the assignments discussed earlier (Figure 1). Interestingly no c-$Li_{15}Si_4$ peak is observed at 0 mV, instead the signal of the small Si cluster phase continuously moves from approximately 8 ppm to an unexpectedly high chemical shift of > 20 ppm during lithiation and moves back to 8 ppm during delithiation on charging from 0 to 116 mV

(see below and Table 2). The maximum shift of this new environment (Figure 5(b), *(iv)*-label) was further investigated with another cell where the cell was discharged below 0 mV until Li metal plating occurred (Figure S7, Supporting Information). A maximum chemical shift of 24 ppm was observed, beyond the values previously reported for electrochemically formed a-Li_xSi. This characteristic high frequency shift derives from a unique a-Li_xSi structural and/or electronic environment, the shift lying outside the normal range expected for diamagnetic lithium environments. The origins of this shift are discussed in more detail below but are ascribed to metallic behavior; on this basis we label this resonance "m-Li_xSi" to denote that it originates from a metallic Li_xSi domain or phase.

d-SiO(1000 °C) The ^7Li NMR spectra are closer to that of a-SiO than that of pure-Si (Figure 5c). However, the maximum shift of the m-Li_xSi peak has increased to 40 ppm in the initial cycle and 30 ppm in the second cycle (Figure 5c, *(iv)*-label). A peak with a fixed chemical shift of 12 ppm was also observed during the first discharge lithiation (Figure 5c, *(v)*-label), similar to that observed for the pure-Si electrode (Figure 5b, *(v)*-label). This appears related to the increased crystalline or ordered Si domain size in the d-SiO, since this peak is characteristic of irreversible dissociation of crystalline Si to amorphous Li_xSi and is not seen in the second discharge.

d-SiO(1100 °C) The ^7Li NMR spectra during initial lithiation show a totally different evolution from that of a-SiO, with the peak with a fixed chemical shift of 12 ppm (Figure 5d, *(v)*-label) along with a very broad m-Li_xSi peak around 40 ppm (Figure 5d, *(iv)*-label) being concurrently observed. The second lithiation more closely resembles that of a-SiO, with a small Si cluster (Figure 1, phase 2) peak that moves from 20 to 10 ppm during the 100 mV process being observed. A peak at 0 ppm, which is attributed to a c-$Li_{15}Si_4$-like structure, now appears towards the end of lithiation. In the initial and second delithiation only a broad peak attributed to residual Li in an extended Si cluster environment is observed (Figure 5d, *(i)*-label), this behavior more closely resembles that seen in pure-Si electrodes.

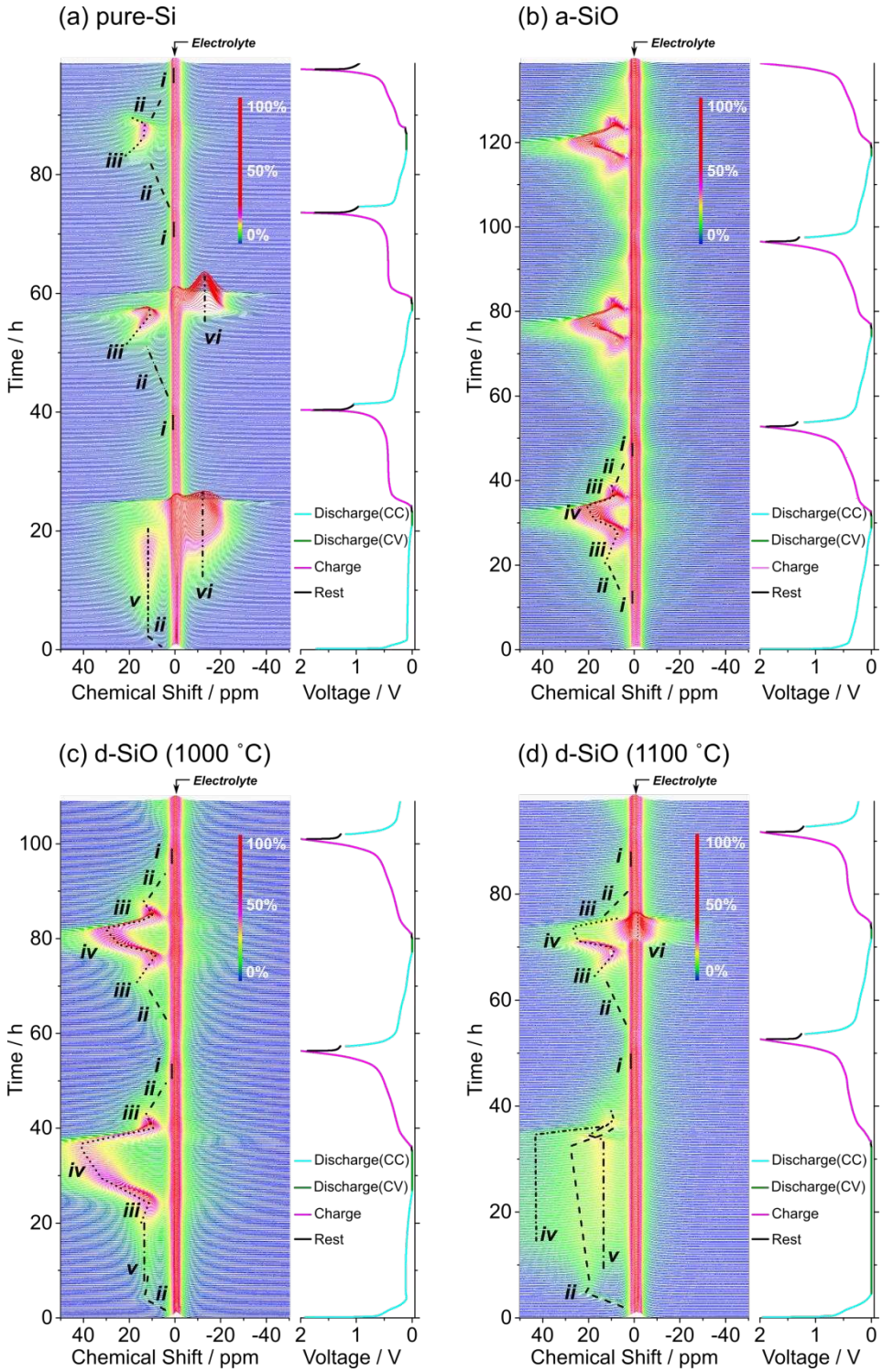

Figure 5. ^{7}Li *in situ* NMR spectra and cell voltage along with measurement time of (a) pure-Si, (b) a-SiO, (c) d-SiO(1000 °C), and (d) d-SiO(1100 °C). The color coding of the NMR intensity is 0% (blue) to 100% (red). The cells have been cycled using constant current discharge at 0.05 C (light blue trace), constant voltage discharge at 0 mV to 0.01 C (green trace) and constant current charge at 0.05 C to 2.0 V (pink trace). There is rest period between each charge and discharge (black trace). The cell was discharged to 100 mV in the third cycle for pure-Si. Li_xSi environments and Li in Super-P/CMC-Na matrix peak are labeled with (*i*) to (*vi*): (*i*) extended Si clusters, phase 1; (*ii*) Li in Super-P / amorphous carbon; (*iii*) small Si clusters, phase 2, (*iv*) m-Li_xSi; (*v*) Li nearby the small Si clusters formed during conversion from crystalline Si to amorphous Li_xSi; (*vi*) c-$Li_{15}Si_4$-like structures, phase 3. Dashed lines have been added as a guide to the eye to indicate when different species or phases are present.

Ex situ ^{7}Li/^{29}Si MAS NMR

Ex situ ^{7}Li and ^{29}Si MAS NMR spectra were recorded to investigate the chemical and electronic structures of electrochemically lithiated a-SiO at various stages of charge and discharge further. For comparison, samples of the lithiated pure-Si electrode were also characterized by *ex situ* ^{7}Li/^{29}Si MAS NMR spectroscopy. A representative set of *ex situ* ^{7}Li MAS NMR spectra during the initial and second lithiation are shown in Figure 6a, the peaks being consistent with the *in situ* ^{7}Li NMR results (Figure 5b), i.e., signals from Li near small Si clusters and in a c-$Li_{15}Si_4$-like structure are seen during the initial lithiation, and three peaks from Li in the three Li_xSi phases are seen during the second lithiation. A small peak is observed at 0 ppm in all spectra often as a shoulder of the stronger Li_xSi signals, which arises from the solid electrolyte interface (SEI) and/or the super-P/CMC-Na matrix.

Figure 6b presents the full set of the *ex situ* ^{29}Si MAS NMR spectra acquired for the pure-Si electrodes of Figure 6a as well as for the micron-sized Si powder. The pristine Si powder gives rise to a narrow ^{29}Si NMR signal at -82 ppm, which corresponds to a crystalline Si environment. This peak disappears completely after the cell has been discharged to 110 mV and is replaced with a broad peak at 50 ppm, which on the basis of the ^{7}Li NMR spectra of the same electrodes (Figure 6a), is ascribed to small Si clusters. After discharging to 60 mV, another peak centered at 750 ppm appears, which is assigned to isolated Si anions; in the fully lithiated state at 0 mV, a broad peak centered around 800 ppm dominates due to an "overlithiated" c-$Li_{15}Si_4$, consistent with earlier ^{29}Si NMR studies.[33] After delithiation to 2.0 V, a ^{29}Si NMR peak at –60 ppm is seen which is noticeably broader than that of c-Si, and is assigned to an a-Si environment (see Figure S6 for the ^{29}Si NMR spectrum of a-Si). The shoulder to higher frequencies is assigned to Si atoms close to residual lithium trapped in the a-Si phase, consistent with the ^{7}Li shift of 6 ppm seen for this phase. For the second lithiation, a broad peak at 0 to 200 ppm is observed for voltages between 230 and 80 mV. The very broad, higher frequency ^{29}Si peaks at approximately 500 ppm (and the associated higher frequency ^{7}Li resonances) may be due to more lithiated parts of the sample, that were not fully delithiated in the 1st charge or they may simply reflect a distribution of local environments. At 60 mV, a very broad peak spanning more than 1000 ppm is observed centered around 400 ppm due to isolated Si anions, on the basis of the corresponding ^{7}Li chemical shift of the same electrodes (Figure 6a). In the fully lithiated state at 0 mV after the second lithiation, the peak center is at around 800 ppm, similar to that seen in the initial cycle. The steady shift to higher frequencies between 80 and 0 mV is ascribed to the crystallization of the Li_xSi phase to form over-lithiated c-$Li_{15}Si_4$. The simplest explanation for a large and positive ^{29}Si shift and a negative shift for ^{7}Li is that the shift originates from a Knight shift in which a band is formed with significant density of states at the Fermi level (E_f) involving Si s orbitals and Li p (rather than s) orbitals. A significant Li 2s contribution to the metallic band structure at E_f would result in a positive shift (see below for further discussion).

In good agreement with the *in situ* ^{7}Li NMR, the *ex situ* ^{7}Li MAS NMR spectra of a-SiO electrodes (Figure 6c) show resonances consistent with Li near extended Si clusters at 230 mV, Li near small Si clusters at 150 and 60 mV and m-Li_xSi in the fully lithiated state at 0 mV. At 420 mV (on the first lithiation) only a peak in the diamagnetic Li region is visible which is present at the same position in all other spectra, appearing as a shoulder of the other stronger Li_xSi signals. This is assigned to the SEI on SiO and Super-P, diamagnetic lithium silicates, and lithiated Super-P carbon.

Figure 6d shows the *ex situ* ^{29}Si MAS NMR spectra of the same a-SiO electrode samples presented in Figure 6c, as well as the pristine a-SiO powder. Tentative assignments are made using the ^{29}Si MAS NMR of the pure-Si electrodes (Figure 6b) and the ^{7}Li NMR of the SiO electrodes (Figure 6c). Pristine a-SiO

exhibits ^{29}Si NMR signals at –108 and –67 ppm, which correspond to silicon dioxide and silicon suboxide (a-Si) environments respectively.[43] Upon lithiation, these signals are replaced by a broad peak shifting from –80 ppm to 120 ppm as the voltage against Li metal drops from 420 mV to 0 mV. However, no broad peak around 600 to 1000 ppm is observed. Upon delithiation to 2.0 V, a ^{29}Si signal at -70 ppm is seen, the shift differing from that of pristine SiO, but lying in the range between a-Si (Figure S6, Supporting Information) and SiO_2,[43] possibly corresponding to a Si sub-oxide/a-Si environment that is different from the pristine material and lithium silicates (see below). For the second lithiation, the acquired spectra are almost the same as those obtained for the initial lithiation. The ^{29}Si chemical shifts ranging from -80 to 120 ppm between 230 and 60 mV correspond initially to extended Si clusters (more negative shifts), small Si clusters, and then eventually at 60 mV where a ^{7}Li resonance at 7 ppm is seen, to Li nearby both isolated Si anions and dimers (note, the ^{29}Si NMR spectra of $Li_{13}Si_7$ contains two resonances between 225 and 342 ppm corresponding to dimers and isolated Si, the exact values vary depending on sample preparation and presumably reflect small differences in Li/Si ratio; surprisingly the higher frequency resonances correspond to the dimers). It is noteworthy that the ^{29}Si chemical shift of a-SiO lithiated to 0 mV, which is associated with a large m-Li_xSi ^{7}Li chemical shift of 20 ppm, also has a ^{29}Si chemical shift of only 120 ppm, which is in the same range as that observed for a Si cluster/isolated Si environment.

A small peak at approximately –70 ppm was also detected, superimposed on the broad ^{29}Si Li_xSi signal in Figure 6d. *Ex situ* ^{29}Si MAS NMR measurements with a narrow frequency range and a longer recycle delay (30 vs. 1 s; Figure 6e) revealed a weak, broad peak at approximately –110 to –120 ppm due to silicon oxides at 420 mV for the initial lithiation, two peaks at –67 ppm and –75 ppm appearing at 230 mV. These two peaks correspond to Li_4SiO_4 and Li_2SiO_3 environments respectively[44] (see also Figure S2 and S3 for Li_4SiO_4, Supporting Information). At 150 mV, the –75 ppm (Li_2SiO_3) peak disappears, with only the –67 ppm (Li_4SiO_4) peak being present at lower potentials. Upon delithiation to 2.0 V, the Li_4SiO_4 peak decreases in intensity and the Li_2SiO_3 peak is recovered to some extent. For the 2nd lithiation, only the Li_4SiO_4 peak is clearly observed below 230 mV. The ^{29}Si MAS NMR results suggest that two different types of species are formed when a-SiO is lithiated, namely Li_xSi and lithium silicates. The change of the lithium silicate signal occurs in the voltage range below 400 mV for lithiation and above 600 mV for delithiation, indicating that the lithium silicates participate, at least partially in the electrochemical reaction. It is important to note that all of the ^{29}Si NMR spectra were acquired under conditions that are not necessarily quantitative, particularly for the diamagnetic phases such as Si, SiO_2 and the lithium silicates, the former phases often having extremely long spin-lattice (T_1) relaxation times of hours; Hahn-echo spectra were also used to acquire the broad spectra. Thus, the observed signals are indicative of the phases present, not their relative phase fractions. T_1 analysis of the 0 mV sample reveals a T_1 of approximately 1 s for the Li_xSi environments and >> 10 s for the Li_4SiO_4-like fractions (Figure S16, Supporting Information). This may be compared to the long T_1 of pure crystalline Li_4SiO_4, 550 s (Figure S17, Supporting Information). A peak at –24 ppm is sometimes observed which may be due to SEI components.[45, 46]

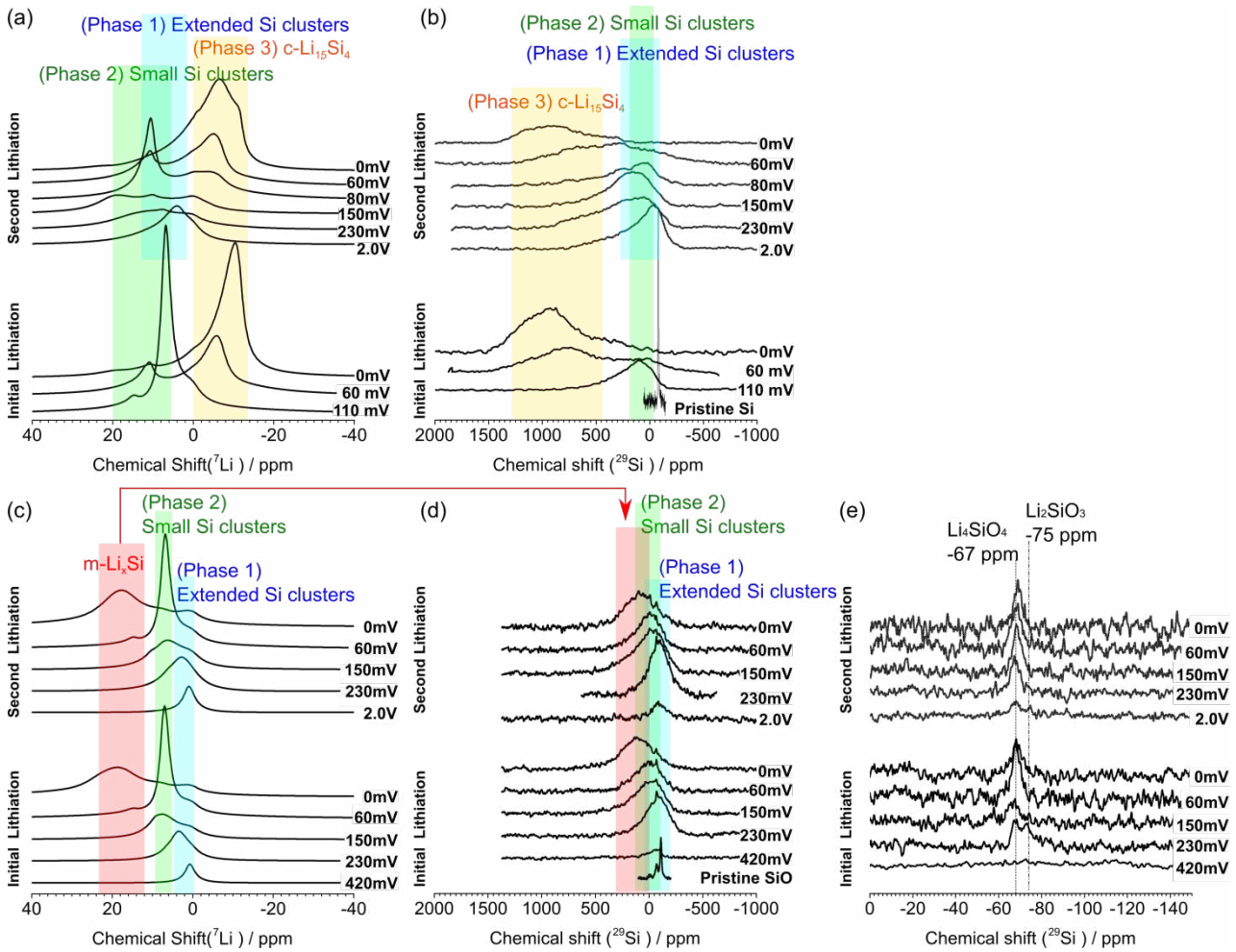

Figure 6. *Ex situ* ^{7}Li MAS NMR single-pulse excitation spectra and ^{29}Si MAS NMR Hahn-echo spectra of lithiated pure-Si (a,b) and a-SiO (c, d, and e), respectively. The ^{29}Si NMR spectra in (b) and (d) have been recorded with a recycle delay of 1 s and ca. 25k scans, whereas the spectra in (e) were recorded with 30 s recycle delay and typically 1k scans. The voltages given next to spectra are the Li-metal half-cell voltage at which the cell was held for at least 24 h before cell disassembly. The color coding of the background highlighting in a, b, c and d indicates the shift range for specific Li_xSi environments; blue represents extended Si clusters, green represents small Si clusters, yellow represents c-$Li_{15}Si_4$-like structure, and red represents m-Li_xSi.

Quantitative analysis of delithiation process of a-SiO

In order to determine the a-SiO reaction pathway, the processes involving SiO must be separated from those originating from the Super-P carbon. The *in situ* ^{7}Li NMR spectra were first deconvoluted at the start and end of the delithiation as well at characteristic inflection points in the dQ/dV profile (Figure S8 and S9, Supporting Information). The different points where NMR spectra were extracted were labeled *a) – i)* in Figure 7A. Another *in situ* NMR experiment was then performed using an electrode containing Super-P/CMC-Na only. The electrochemistry and spectra were analyzed at five stages corresponding those seen for the full electrode, *a)*, *b)*, *d)*, *g)*, *h)* and *i)* (Figure S10 and Table S2, Supporting Information) allowing the location of the peaks due to lithiated Super-P to be identified and the Li content of this matrix at each state of charge to be determined. The amount of Li involved in the delithiation processes of the a-SiO component of the full electrode was then estimated from the electrochemical profile of the full

electrode, taking into account the Li fraction in the Super-P/CMC-Na component at each state of charge (Table 2). From *a)* to *b)* m-Li_xSi peak shift position returns to that corresponding to that assigned to the small Si clusters/isolated Si, the capacity of this process (and change in associated lithiated content of the electrode) being determined from the electrochemistry (Table 2). In the same way, the capacity of *b)* to *d)* is assigned to the growth of more small Si clusters (such as dimers) by reaction of the isolated Si anions, and from *d)* to *g)* to the formation and growth of more extended Si clusters on removal of Li. From *g)* to *h)*, there is small reduction in intensity of the diamagnetic Li peak at 1 ppm. This change is ascribed to the (partial) delithiation of Li_4SiO_4. From *h)* to *i)* a small change in intensity of extended Si cluster peak is seen, indicating that higher voltages are required to pull the last remaining Li ions out of the extended Si, a-Li_xSi matrix. Although the total change in NMR intensities determined by NMR line shape deconvolution (Figure 7B) is qualitatively consistent with the numbers reported in Table 2, the Li_xSi capacity of each stage as determined by NMR is less accurate in regions where there is significant overlap between the Super-P Li and Li_xSi signals (e.g., region a) – b); see Table S4, Supporting Information for more detailed analysis). Furthermore, due to the short recycle delays used to acquire the ^7Li spectra, it is difficult to extract quantitative values for the changes in the concentrations of species assigned to the peak centered at 1 ppm, i.e., the lithium silicate phase(s) and multiple peaks from the electrolyte and SEI.

Table 2. Li concentrations involved in specific parts of the first delithiation process of a-SiO electrode estimated from the electrochemical analysis and standardized by molar equivalent of SiO in the electrode. The capacity of Super-P/CMC-Na matrix in the a-SiO electrode was estimated from an electrochemical measurement of a Super-P/CMC-Na electrode performed in a separate experiment (Figure S10 and Table S2, Supporting Information), the values given in the table being adjusted to account for the phase fraction of Super-P/CMC-Na in the composite electrode. The Li content in a-SiO was then determined and assigned to specific phases based on the Li NMR experiments.

Stage	Overall change in Li content in electrode during each stage (mol per SiO)	Super-P/CMC-Na (mol per SiO)	a-SiO (mol per SiO)	Source of Li
a) – b)	0.16	0.13	0.03	m-Li_xSi
b) – d)	1.39	0.12	1.27	Li_xSi (small Si clusters)
d) – g)	1.20	0.07	1.13	Li_xSi (extended Si clusters)
g) – h)	0.22	0.03	0.19	Lithium silicate
h) – i)	0.17	0.02	0.15	Li_xSi (extended Si clusters)
Total Li capacity	3.14	0.37	2.77	

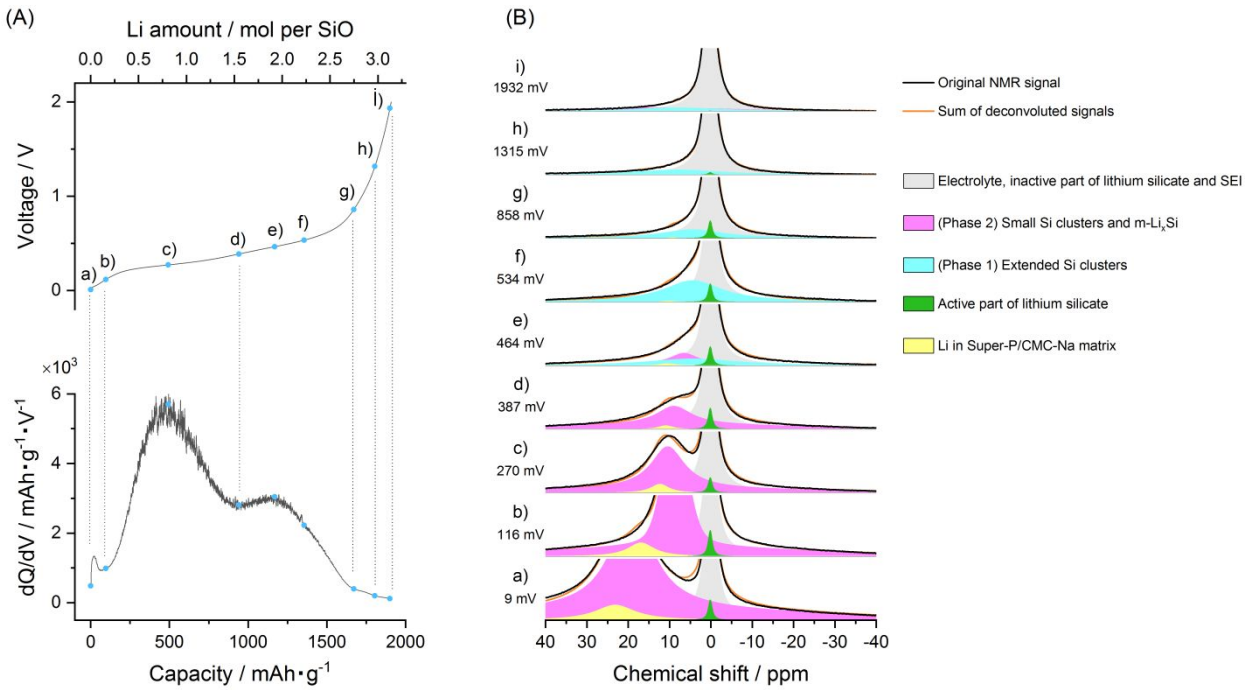

Figure 7. (A)Voltage-Li amount profile and dQ/dV—capacity profile of initial delithiation of a-SiO. (B) Extracted scans taken from the *in situ* ^{7}Li NMR spectra of a-SiO and the deconvoluted resonances. The points in the electrochemistry where slices in the *in situ* NMR spectra were taken are indicated in the voltage-Li amount profile and labeled a) – i) in (A). The Super-P/CMC-Na signal intensity and position was constrained based on the fits performed on the *in situ* ^{7}Li NMR spectra of a Super-P/CMC-Na electrode. Deconvolution parameters in used DMFIT are found in Table S3 (Supporting information).

Lithiation/delithiation reaction model for SiO

The lithiation/delithiation reaction of crystalline c-Si and a-SiO can be described by equations (1) – (2) and (3) – (4), respectively, based on the observed chemical shifts in *in situ* ^{7}Li NMR and *ex situ* ^{7}Li/^{29}Si MAS NMR measurements (Scheme 1). Pure-Si, which is crystalline before lithiation, is converted to amorphous Li_xSi (small Si clusters) in its initial lithiation and a c-$Li_{15}Si_4$-like structure in its fully lithiated state (Scheme 1, Eq. (1)). The c-$Li_{15}Si_4$ is delithiated to form amorphous Li_xSi (with extended Si clusters) during the delithiation and a-Si in its fully delithiated state. In the subsequent lithiation/delithiation, conversion between a-Si/Li_xSi and c-$Li_{15}Si_4$ is repeated (Scheme 1, Eq. (2)). Li_xSi is the only electrochemically active phase during reactions of c-Si.

In contrast to that, a-SiO has two electrochemically active phases, Li_xSi and a lithium silicate phase, the latter being formed during the first lithiation. The Si domain in a-SiO is converted to Li_xSi while at the same time, the SiO_2 and sub-oxide components partially phase separate to form Li_xSi and lithium silicates. During lithiation, the Li_xSi is converted to m-Li_xSi via extended Si clusters and small Si clusters; at the same time, the SiO_2 component is almost completely lithiated to form Li_4SiO_4 [Scheme 1, Eq. (3 and 3a, 3b, 3c)]. In the delithiation process, Li_xSi and small fraction of the Li_4SiO_4 is delithiated to silicon sub-oxide and Li_2SiO_3 through Li_xSi (extended Si clusters) and Li_xSi (small Si clusters) (Table 2). Almost all Li in the in Li_xSi phase formed from a-SiO is extracted at 2.0 V (Figure 7A, i)-label); the analysis reported in Table 2 shows that the total Li capacity per formula unit of SiO is 2.77, which includes 0.19 Li from lithium silicate phase, thus this corresponds to 2.58 Li from Li_xSi per formula unit of SiO. Furthermore, since from Eq. (3) in Scheme 1, 75% of the silicon atoms in SiO are transformed to Li_xSi, x in the fully

lithiated state corresponds to approximately 3.44. Only 0.19 Li are removed per formula unit of SiO from the Li_4SiO_4 phase after delithiation and thus considerable Li_4SiO_4 remains, the Li in this phase accounting at least in part for some the irreversible capacity in the 1st cycle. Thus, the delithiated state consist of multiple phases, namely Li_4SiO_4, Li_2SiO_3 and Si sub-oxide. In the subsequent lithiation/delithiation, conversion between Li_xSi/Li_4SiO_4 and Si sub-oxide/Li_4SiO_4/Li_2SiO_3 is repeated (Scheme 1, Eq. (3 to 5)). The overall delithiation reaction is reported in Eq. 5 in Scheme 1, where all the Li_2SiO_3 is presumed to have reacted to simplify the equation, and the Si sub-oxide is written as Si + SiO_2.

Crystalline Si (c-Si)

Initial lithiation

$$4\,c\text{–}Si \xrightarrow{Li^+,e^-} 4\,a\text{–}Li_xSi \xrightarrow{Li^+,e^-} c\text{–}Li_{15}Si_4 \qquad \text{Eq. (1)}$$

Subsequent lithiation/delithiation

$$c\text{–}Li_{15}Si_4 \xleftrightarrow{Li^+,e^-} 4\,a\text{–}Li_xSi \xleftrightarrow{Li^+,e^-} 4\,a\text{–}Si \qquad \text{Eq. (2)}$$

Amorphous silicon monoxide (a-SiO)

Initial lithiation

$$4SiO \xrightarrow{Li^+,e^-} Li_4SiO_4 + 3\,a\text{–}Li_xSi \qquad \text{Eq. (3)}$$

$$a\text{–}Si \xrightarrow{Li^+,e^-} a\text{–}Li_xSi \qquad \text{Eq. (3a)}$$

$$SiO_2 \xrightarrow{Li^+,e^-} Li_4SiO_4 + a\text{–}Li_xSi \qquad \text{Eq. (3b)}$$

$$SiO_{y<2} \xrightarrow{Li^+,e^-} \tfrac{y}{4}Li_4SiO_4 + \left(1-\tfrac{y}{4}\right)a\text{–}Li_xSi \qquad \text{Eq. (3c)}$$

(Subsequent lithiation/delithiation)

$$Li_4SiO_4 + 3\,a\text{–}Li_xSi \xleftrightarrow{Li^+,e^-} (1-z)Li_4SiO_4 + zLi_2SiO_3 + 3SiO_{z/3} \qquad \text{Eq. (4)}$$

or, for x = 3.44

$$0.25\,Li_4SiO_4 + 0.75\,Li_{3.44}Si \leftrightarrow 2.77\,Li + 0.40\,SiO_2 + 0.20\,Li_4SiO_4 + 0.40\,Si \qquad \text{Eq. (5)}$$

Scheme 1. Reaction model for crystalline silicon (c-Si) and amorphous silicon monoxide (a-SiO) derived from solid-state NMR spectroscopy. For SiO, Eq. (3) represents the overall reaction. Since SiO comprises 3 components, a-Si, SiO_2 and the interfacial environments, $SiO_{\alpha<2}$, Eq. (3) can be subdivided into three separate reactions (3a – c), where $SiO_{y<0}$ simply represents the interface or interphase between the Si and SiO_2 components. Eq. 5 has been evaluated assuming that the oxygen atoms in Li_4SiO_4 react with additional silicon atoms from Li_xSi to form Si and SiO_2, using the quantification outlined in Table 2.

DISCUSSION

In situ ^{7}Li NMR revealed different lithiation/delithiation pathways for a-SiO and pure-Si electrodes, with the former varying as a function of heat treatment of the starting material. Lithiation of crystalline Si is characterized by asymmetric electrochemistry and *in situ* NMR spectra and by the observation of c-$Li_{15}Si_4$. By contrast, the characteristics of a-SiO are a symmetrical and sloping voltage/capacity profile representing two solid solution processes similar to those seen for phase 1 and 2 (Figure 1) for c-Si; but in contrast to c-Si no c-$Li_{15}Si_4$ formation/removal is observed below 100 mV. A small amount of capacity is nonetheless observed below 116 mV (Table 2, Figure 7) indicating that phase 2 can be lithiated further. The NMR spectra are consistent with this: the ^{7}Li NMR shifts on charge mirror those on discharge over multiple lithiation/delithiation cycles. No c-$Li_{15}Si_4$ peak is seen; instead a new ^{7}Li resonance (m-Li_xSi) that shifts to a higher frequency than that of phase 2 from 116 to 0 V is observed. This significant shift, from 20 to 10 ppm on delithiation is associated with only a very small compositional change of the Li_xSi phase, from $Li_{3.44}Si$ to only $Li_{3.40}Si$ (Table 2 and Scheme 1).

Qualitatively similar NMR spectra were obtained for d-SiO(1000 °C) which has a c-Si domain size of 3.1(2) nm, but notably a larger shift was observed for the m-Li_xSi resonance, the resonance now shifting asymmetrically to 40 ppm on the first discharge and 30 ppm on the second discharge. The larger shift between the first and second discharge, and compared to that observed for a-SiO, is correlated with higher capacity below 100 mV (Figure S18, Supporting Information). Note that a plateau is observed on the first lithiation, which is characteristic of the breakup of the crystalline Si network. The observation of this plateau does not however correlate with $Li_{15}Si_4$ formation. Electrochemical signatures of the c-$Li_{15}Si_4$ phase are observed on increasing the c-Si domain size to 5.0(1) nm in d-SiO(1100 °C). However, the NMR spectra of d-SiO(1100 °C) reveal behavior that is intermediate between that of d-SiO(1000 °C) and c-Si: the m-Li_xSi environment is still observed (more clearly in the 2nd cycle), shifting to over 20 ppm along with the signal from c-$Li_{15}Si_4$ which now appears at –6 ppm (as opposed to –13 ppm for c-Si).

The ^{29}Si resonance observed in the *ex situ* MAS NMR spectrum of the a-SiO m-Li_xSi phase in its fully lithiated state has a ^{29}Si shift that is only slightly larger than that observed for Si environments in the extended cluster (phase 1) and small Si cluster (phase 2) phases, noticeably less than that of the "overlithiated" c-$Li_{15}Si_4$ phase. In contrast m-Li_xSi has large positive ^{7}Li shift. A range of ^{6,7}Li shifts have been observed for the high Li-content lithium silicides with isolated silicon anions, with stoichiometric $Li_{15}Si_4$ resonating at 8 to 10 ppm,[47, 48], $Li_{4.11}Si$ ($Li_{16.42}Si_4$) at 63 ppm,[47], $Li_{21}Si_5$ at 70.5 and 93.7 ppm[33] and the closely related phase, $Li_{17}Si_4$ at 76.5 and 119 ppm,[49]. In their theoretical analysis of these phases,[50, 51] Fässler *et al.* describe $Li_{15}Si_4$ as a p-doped semiconductor, with a band gap above the Fermi level, E_f; no such band gap existing in the higher Li content lithium silicides. The bands near the Fermi level are formed by Si 3p not 3s orbitals (and Li s/p orbitals), and so naively, large positive Knight shifts are not necessarily predicted. The large ^{7}Li shift seen for m-Li_xSi is, however, ascribed to increasing metallic behavior, corresponding to a Knight shift, the Li 2s orbitals presumably contributing to the density of states at E_f. The small ^{29}Si shift is consistent with the involvement of both 3s and 3p orbitals at E_f. This is in contrast to the behavior of "$Li_{15+x}Si_4$" where a negative shift was observed which appears to suggest Li 2p character at E_f. However, large ^{7}Li and ^{29}Si chemical shifts are also expected in these (semi)metallic Li_xSi systems, with small or zero bandgaps, which complicates the NMR analysis. This behavior differs from that observed following partial substitution of the Li in $Li_{15}Si_4$ by Mg and Al; this increases the electron doping, and results in increased positive Li Knight Shift, suggesting that the Li 2s orbitals are involved.

Careful structural analysis of $Li_{15}Si_4$ shows that there are two fully occupied Li crystallographic sites[50, 51]

and so it is not immediately clear where any additional Li would be located. Negative shifts were also observed for $Li_{15}Ge_4$ in *ex situ* ^{7}Li NMR studies of germanium batteries at –13 and –58 ppm, which based on their relative intensities were assigned to the 48*e* and 12*a* sites respectively in the $Cu_{15}Si_4$ structure type (adopted by both the Ge and Si phases). A resonance at an intermediate position (−20 ppm) was often observed during *in situ* NMR experiments, likely representing a dynamic average of the Li on the 48*e* and 12*a* sites.[52] What is clear is that $Li_{15}Si_4$ tolerates a degree of non-stoichiometry which has a significant effect on its electronic properties. However, it remains unclear as to whether the negative shift seen electrochemically corresponds to $Li_{15+x}Si_4$, where $x > 0$ or whether the phase formed electrochemically corresponds to x = 0, and the phase formed on delithiation corresponds to $x < 0$.

a-SiO with a-Si domains forms an amorphous yet metallic phase. Comparing the electrochemistry of all d-SiOs, which have different Si domain size, it is clear that the domain size of Si in the pristine material determines whether a c-$Li_{15}Si_4$-like phase is formed at the end of the lithiation, domain sizes of > 3 nm being required. Even when 5 nm Si particles are present, the behavior differs from that of the bulk phase, the most lithiated phase resonating at 0 ppm. Furthermore, this phase is only formed on holding at 0 V. There are two possible explanations for this "overpotential". The first is kinetic in origin and is associated with the reduced ionic and electronic transport through the SiO_2 (and Li_4SiO_4) coating that surrounds the Si domains. The second is thermodynamic and may be associated with a clamping effect of the matrix. For example, Obrovac *et al.* have shown that $Li_{15}Si_4$ does not form for Si thin films tightly bonded to a substrate, due to compressive stress.[4, 53] It is thus possible that the SiO_2 (and Li_4SiO_4) matrix may also result in similar compressive stresses.

The continuous structural transformations (rather than two-phase reactions) in a-SiO are likely a significant mechanism for suppressing crack formation caused by particle volume change during lithiation/delithiation, resulting in one reason for the improved cyclability of a-SiO compared with pure-Si. The "domain size stabilizer", i.e. lithium silicate phase, is partially electrochemical active. From *ex situ* ^{29}Si MAS NMR, the lithiated state is Li_4SiO_4 and delithiated state is mixture of Li_4SiO_4 and Li_2SiO_3. Since Li_4SiO_4 was reported previously to be electrochemically inactive,[54] the amorphous nature or the nano-domain structure of Li_4SiO_4 in the a-SiO matrix may impart some reactivity to the lithium silicate phase. We confirmed that mechano-chemically synthesized amorphous Li_4SiO_4 reacts to form Li_2SiO_3 after subsequent lithiation and delithiation, although the specific capacity is much lower than calculated for the lithium silicate part of a-SiO electrodes (Figure S4 and S5, Supporting Information). It is likely that the domain size stabilizer effect of the lithium silicate phase is retained because the delithiation is only partially complete and Li_2SiO_3 rather than SiO_2 is formed. As this lithium silicate phase reaction results in an irreversible capacity, an understanding of this phenomenon is also important for designing commercial LIBs.

CONCLUSION

The reaction of SiO active material for LIBs was investigated using *in situ* ^{7}Li NMR and *ex situ* ^{7}Li/^{29}Si MAS NMR. Two different types of phases are found during lithiation, Li_xSi and lithium silicates, both of which are electrochemically active. The fully lithiated state of a-SiO consists of Li_4SiO_4 and a characteristic Li_xSi environment due to metallic domains, which has a relatively high lithium concentration of 3.45 Li per Si, but yet does not undergo a phase transition to a c-$Li_{15}Si_4$-like structure. Instead the lithiation/delithiation pathway occurs via gradual solid solution processes involving amorphous phases. This is in contrast to pure-Si, which forms c-$Li_{15}Si_4$ in its fully lithiated state via a two-phase reaction. The symmetrical and gradual phase transition via solid solution in a-SiO, without the formation of c-$Li_{15}Si_4$, is likely to be key to its improved cyclability, as crack formation inside the particles is prevented. A second cause of the good cyclability of the a-SiO derives from well separated nano-sized Si domains surrounded by SiO_2 regions. This results in nano-domains of Li_xSi surrounded by Li_4SiO_4 on lithiation. These oxide-containing (SiO_2 and $SiO_{x<2}$) buffer layers prevent the a-Si domains from sintering (growing larger) on cycling and also most likely help suppress the continual SEI formation that occurs in pure-Si.

In situ ^{7}Li NMR measurements of d-SiO electrodes revealed that the size and crystallinity of the Si domains in heat treated SiO can play a crucial role in controlling the overpotential associated with the break-up of the crystalline Si domains on the first cycle, as well as determining whether c-$Li_{15}Si_4$ is formed or not in the fully lithiated state. The identification of a characteristic high lithium concentration metallic Li_xSi phase linked to good cyclability of the SiO, as well as the crucial role played by the size of Si domains in controlling the phase evolution, offers crucial insights for the design of future Si based anodes that combine high capacity with a long cycle-life.

ASSOCIATED CONTENT

Supporting Information

The Supporting Information is available free of charge on the ACS Publications website at DOI: TBA. Contents:

- Reaction schemes with SiO-based negative anodes
- Synthesis and characterization of Li_4SiO_4 and a-Si by XRD and $^{1}H/^{7}Li/^{29}Si$ MAS NMR
- *In situ* ^{7}Li NMR experiments and related data
- Capacity estimated from *in situ* ^{7}Li NMR and electrochemical analysis
- Rietveld refinements
- ^{29}Si MAS NMR and T_1 experiments
- Capacity— and dQ/dV—voltage profile for a-SiO and d-SiO(1000 °C) during ^{7}Li *in situ* NMR

AUTHOR INFORMATION

Corresponding Author

*E-mail cpg27@cam.ac.uk (C.P.G.)

Notes

The authors declare no competing financial interest.

ORCID

Clare P. Grey: 0000-0001-5572-192X

Keitaro Kitada: 0000-0001-8372-2508

Pieter C.M.M. Magusin: 0000-0003-1167-3764

Matthias F. Groh: 0000-0002-7436-7177

Robert S. Weatherup: 0000-0002-3993-9045

ACKNOWLEDGEMENTS

We gratefully acknowledge the help of Joshua M. Stratford (Cambridge, UK) during *in situ* NMR data handling. This project has received funding from the European Union's Horizon 2020 research and innovation program under the EU Marie Skłodowska-Curie grant numbers 655444 (O.P.) and 656870 (R.S.W.), Sony corporation and "Sony Energy Devices corporation educational program" (K.K.), the Engineering and Physical Sciences Research Council (EPSRC Grant No: EP/P003532/1) (M.F.G.), and the German Research Foundation (DFG, Research Fellowship GR 5342/1-1 for M.F.G.).

REFERENCES

1. Deng, D., Li-ion batteries: basics, progress, and challenges. *Energy Science & Engineering* **2015,** *3* (5), 385-418.
2. Ohzuku, T., Formation of Lithium-Graphite Intercalation Compounds in Nonaqueous Electrolytes and Their Application as a Negative Electrode for a Lithium Ion (Shuttlecock) Cell. *Journal of The Electrochemical Society* **1993,** *140* (9).
3. Obrovac, M. N.; Chevrier, V. L., Alloy negative electrodes for Li-ion batteries. *Chem Rev* **2014,** *114* (23), 11444-502.
4. Iaboni, D. S. M.; Obrovac, M. N., $Li_{15}Si_4$Formation in Silicon Thin Film Negative Electrodes. *Journal of The Electrochemical Society* **2015,** *163* (2), A255-A261.
5. Fuchsbichler, B.; Stangl, C.; Kren, H.; Uhlig, F.; Koller, S., High capacity graphite–silicon composite anode material for lithium-ion batteries. *Journal of Power Sources* **2011,** *196* (5), 2889-2892.
6. Obrovac, M. N.; Christensen, L., Structural Changes in Silicon Anodes during Lithium Insertion/Extraction. *Electrochemical and Solid-State Letters* **2004,** *7* (5).
7. Tranchot, A.; Etiemble, A.; Thivel, P. X.; Idrissi, H.; Roué, L., In-situ acoustic emission study of Si-based electrodes for Li-ion batteries. *Journal of Power Sources* **2015,** *279*, 259-266.
8. Liu, X. H.; Zhong, L.; Huang, S.; Mao, S. X.; Zhu, T.; Huang, J. Y., Size-dependent fracture of silicon nanoparticles during lithiation. *ACS Nano* **2012,** *6* (2), 1522-31.
9. Ogata, K.; Salager, E.; Kerr, C. J.; Fraser, A. E.; Ducati, C.; Morris, A. J.; Hofmann, S.; Grey, C. P., Revealing lithium-silicide phase transformations in nano-structured silicon-based lithium ion batteries via in situ NMR spectroscopy. *Nat Commun* **2014,** *5*, 3217.
10. Zhang, Y.; Zhang, X. G.; Zhang, H. L.; Zhao, Z. G.; Li, F.; Liu, C.; Cheng, H. M., Composite anode material of silicon/graphite/carbon nanotubes for Li-ion batteries. *Electrochimica Acta* **2006,** *51* (23), 4994-5000.
11. Dimov, N.; Kugino, S.; Yoshio, M., Mixed silicon–graphite composites as anode material for lithium ion batteries. *Journal of Power Sources* **2004,** *136* (1), 108-114.
12. Khomenko, V. G.; Barsukov, V. Z.; Doninger, J. E.; Barsukov, I. V., Lithium-ion batteries based on carbon–silicon–graphite composite anodes. *Journal of Power Sources* **2007,** *165* (2), 598-608.
13. Hochgatterer, N. S.; Schweiger, M. R.; Koller, S.; Raimann, P. R.; Wöhrle, T.; Wurm, C.; Winter, M., Silicon/Graphite Composite Electrodes for High-Capacity Anodes: Influence of Binder Chemistry on Cycling Stability. *Electrochemical and Solid-State Letters* **2008,** *11* (5).
14. Miyuki, T.; Okuyama, Y.; Sakamoto, T.; Eda, Y.; Kojima, T.; Sakai, T., Characterization of Heat Treated SiO Powder and Development of a $LiFePO_4$/SiO Lithium Ion Battery with High-Rate Capability and Thermostability. *Electrochemistry* **2012,** *80* (6), 401-404.
15. Hirata, A.; Kohara, S.; Asada, T.; Arao, M.; Yogi, C.; Imai, H.; Tan, Y.; Fujita, T.; Chen, M., Atomic-scale disproportionation in amorphous silicon monoxide. *Nat Commun* **2016,** *7*, 11591.
16. Mamiya, M.; Takei, H.; Kikuchi, M.; Uyeda, C., Preparation of fine silicon particles from amorphous silicon monoxide by the disproportionation reaction. *Journal of Crystal Growth* **2001,** *229* (1-4), 457-461.
17. Yasaitis, J. A.; Kaplow, R., Structure of Amorphous Silicon Monoxide. *Journal of Applied Physics* **1972,** *43* (3), 995-1000.

18. Miyachi, M.; Yamamoto, H.; Kawai, H.; Ohta, T.; Shirakata, M., Analysis of SiO Anodes for Lithium-Ion Batteries. *Journal of The Electrochemical Society* **2005,** *152* (10).

19. Morita, T.; Takami, N., Nano Si Cluster-SiOx-C Composite Material as High-Capacity Anode Material for Rechargeable Lithium Batteries. *Journal of The Electrochemical Society* **2006,** *153* (2).

20. Kim, J.-H.; Sohn, H.-J.; Kim, H.; Jeong, G.; Choi, W., Enhanced cycle performance of SiO-C composite anode for lithium-ion batteries. *Journal of Power Sources* **2007,** *170* (2), 456-459.

21. Kim, J.-H.; Park, C.-M.; Kim, H.; Kim, Y.-J.; Sohn, H.-J., Electrochemical behavior of SiO anode for Li secondary batteries. *Journal of Electroanalytical Chemistry* **2011,** *661* (1), 245-249.

22. Yamada, M.; Inaba, A.; Ueda, A.; Matsumoto, K.; Iwasaki, T.; Ohzuku, T., Reaction Mechanism of "SiO"-Carbon Composite-Negative Electrode for High-Capacity Lithium-Ion Batteries. *Journal of The Electrochemical Society* **2012,** *159* (10), A1630-A1635.

23. Takezawa, H.; Iwamoto, K.; Ito, S.; Yoshizawa, H., Electrochemical behaviors of nonstoichiometric silicon suboxides (SiO_x) film prepared by reactive evaporation for lithium rechargeable batteries. *Journal of Power Sources* **2013,** *244*, 149-157.

24. Yu, B.-C.; Hwa, Y.; Park, C.-M.; Sohn, H.-J., Reaction mechanism and enhancement of cyclability of SiO anodes by surface etching with NaOH for Li-ion batteries. *Journal of Materials Chemistry A* **2013,** *1* (15).

25. Kim, K. W.; Park, H.; Lee, J. G.; Kim, J.; Kim, Y.-U.; Ryu, J. H.; Kim, J. J.; Oh, S. M., Capacity variation of carbon-coated silicon monoxide negative electrode for lithium-ion batteries. *Electrochimica Acta* **2013,** *103*, 226-230.

26. Yom, J. H.; Hwang, S. W.; Cho, S. M.; Yoon, W. Y., Improvement of irreversible behavior of SiO anodes for lithium ion batteries by a solid state reaction at high temperature. *Journal of Power Sources* **2016,** *311*, 159-166.

27. Yasuda, K.; Kashitani, Y.; Kizaki, S.; Takeshita, K.; Fujita, T.; Shimosaki, S., Thermodynamic analysis and effect of crystallinity for silicon monoxide negative electrode for lithium ion batteries. *Journal of Power Sources* **2016,** *329*, 462-472.

28. Huang, T.; Yang, Y.; Pu, K.; Zhang, J.; Gao, M.; Pan, H.; Liu, Y., Linking particle size to improved electrochemical performance of SiO anodes for Li-ion batteries. *RSC Advances* **2017,** *7* (4), 2273-2280.

29. Hirose, T.; Morishita, M.; Yoshitake, H.; Sakai, T., Study of structural changes that occurred during charge/discharge of carbon-coated SiO anode by nuclear magnetic resonance. *Solid State Ionics* **2017,** *303*, 154-160.

30. Nagao, Y.; Sakaguchi, H.; Honda, H.; Fukunaga, T.; Esaka, T., Structural Analysis of Pure and Electrochemically Lithiated SiO Using Neutron Elastic Scattering. *Journal of The Electrochemical Society* **2004,** *151* (10).

31. Hwa, Y.; Park, C.-M.; Sohn, H.-J., Modified SiO as a high performance anode for Li-ion batteries. *Journal of Power Sources* **2013,** *222*, 129-134.

32. Park, C.-M.; Choi, W.; Hwa, Y.; Kim, J.-H.; Jeong, G.; Sohn, H.-J., Characterizations and electrochemical behaviors of disproportionated SiO and its composite for rechargeable Li-ion batteries. *Journal of Materials Chemistry* **2010,** *20* (23).

33. Key, B.; Bhattacharyya, R.; Morcrette, M.; Seznec, V.; Tarascon, J. M.; Grey, C. P., Real-time NMR investigations of structural changes in silicon electrodes for lithium-ion batteries. *J Am Chem Soc* **2009,** *131* (26), 9239-49.

34. Key, B.; Morcrette, M.; Tarascon, J. M.; Grey, C. P., Pair distribution function analysis and solid state NMR studies of silicon electrodes for lithium ion batteries: understanding the (de)lithiation mechanisms. *J Am Chem Soc*

2011, *133* (3), 503-12.

35. Koster, T. K.; Salager, E.; Morris, A. J.; Key, B.; Seznec, V.; Morcrette, M.; Pickard, C. J.; Grey, C. P., Resolving the different silicon clusters in $Li_{12}Si_7$ by ^{29}Si and $^{6,7}Li$ solid-state NMR spectroscopy. *Angew Chem Int Ed Engl* **2011,** *50* (52), 12591-4.

36. Pecher, O.; Bayley, P. M.; Liu, H.; Liu, Z.; Trease, N. M.; Grey, C. P., Automatic Tuning Matching Cycler (ATMC) in situ NMR spectroscopy as a novel approach for real-time investigations of Li- and Na-ion batteries. *J Magn Reson* **2016,** *265*, 200-9.

37. Pecher, O.; Carretero-González, J.; Griffith, K. J.; Grey, C. P., Materials' Methods: NMR in Battery Research. *Chemistry of Materials* **2016,** *29* (1), 213-242.

38. Coelho, A., Topas 4.1. *Coelho Software: Brisbane, Australia* **2007**.

39. Balzar, D.; Audebrand, N.; Daymond, M. R.; Fitch, A.; Hewat, A.; Langford, J. I.; Le Bail, A.; Louër, D.; Masson, O.; McCowan, C. N.; Popa, N. C.; Stephens, P. W.; Toby, B. H., Size–strain line-broadening analysis of the ceria round-robin sample. *Journal of Applied Crystallography* **2004,** *37* (6), 911-924.

40. Massiot, D.; Fayon, F.; Capron, M.; King, I.; Le Calvé, S.; Alonso, B.; Durand, J.-O.; Bujoli, B.; Gan, Z.; Hoatson, G., Modelling one- and two-dimensional solid-state NMR spectra. *Magnetic Resonance in Chemistry* **2002,** *40* (1), 70-76.

41. d'Amour, H.; Denner, W.; Schulz, H., Structure determination of α-quartz up to 68 x 108 Pa. *Acta Crystallographica Section B Structural Crystallography and Crystal Chemistry* **1979,** *35* (3), 550-555.

42. Többens, D. M.; Stüßer, N.; Knorr, K.; Mayer, H. M.; Lampert, G., E9: The New High-Resolution Neutron Powder Diffractometer at the Berlin Neutron Scattering Center. *Materials Science Forum* **2001,** *378-381*, 288-293.

43. Friede, B.; Jansen, M., Some comments on so-called 'silicon monoxide'. *Journal of Non-Crystalline Solids* **1996,** *204* (2), 202-203.

44. de Jong, B. H. W. S.; Supèr, H. T. J.; Spek, A. L.; Veldman, N.; Nachtegaal, G.; Fischer, J. C., Mixed Alkali Systems: Structure and ^{29}Si MASNMR of $Li_2Si_2O_5$ and $K_2Si_2O_5$. *Acta Crystallographica Section B Structural Science* **1998,** *54* (5), 568-577.

45. Jin, Y.; Kneusels, N. H.; Magusin, P.; Kim, G.; Castillo-Martinez, E.; Marbella, L. E.; Kerber, R. N.; Howe, D. J.; Paul, S.; Liu, T.; Grey, C. P., Identifying the Structural Basis for the Increased Stability of the Solid Electrolyte Interphase Formed on Silicon with the Additive Fluoroethylene Carbonate. *J Am Chem Soc* **2017,** *139* (42), 14992-15004.

46. Jin, Y.; Kneusels, N. H.; Marbella, L. E.; Castillo-Martinez, E.; Magusin, P.; Weatherup, R. S.; Jonsson, E.; Liu, T.; Paul, S.; Grey, C. P., Understanding Fluoroethylene Carbonate and Vinylene Carbonate Based Electrolytes for Si Anodes in Lithium Ion Batteries with NMR Spectroscopy. *J Am Chem Soc* **2018,** *140* (31), 9854-9867.

47. Baran, V.; van Wullen, L.; Fassler, T. F., Substitution of Lithium for Magnesium, Zinc, and Aluminum in $Li_{15}Si_4$: Crystal Structures, Thermodynamic Properties, as well as ^6Li and ^7Li NMR Spectroscopy of $Li_{15}Si_4$ and $Li_{15-x}M_xSi_4$ (M=Mg, Zn, and Al). *Chemistry* **2016,** *22* (19), 6598-609.

48. Dupke, S.; Langer, T.; Pottgen, R.; Winter, M.; Passerini, S.; Eckert, H., Structural characterization of the lithium silicides $Li_{15}Si_4$, $Li_{13}Si_4$, and Li_7Si_3 using solid state NMR. *Phys Chem Chem Phys* **2012,** *14* (18), 6496-508.

49. Zeilinger, M.; Benson, D.; Häussermann, U.; Fässler, T. F., Single Crystal Growth and Thermodynamic Stability of $Li_{17}Si_4$. *Chemistry of Materials* **2013,** *25* (9), 1960-1967.

50. Zeilinger, M.; Kurylyshyn, I. M.; Häussermann, U.; Fässler, T. F., Revision of the Li–Si Phase Diagram: Discovery and Single-Crystal X-ray Structure Determination of the High-Temperature Phase $Li_{4.11}Si$. *Chemistry of Materials* **2013,** *25* (22), 4623-4632.

51. Zeilinger, M.; Baran, V.; van Wüllen, L.; Häussermann, U.; Fässler, T. F., Stabilizing the Phase $Li_{15}Si_4$ through Lithium–Aluminum Substitution in $Li_{15-x}Al_xSi_4$ ($0.4 < x < 0.8$)—Single Crystal X-ray Structure Determination of $Li_{15}Si_4$ and $Li_{14.37}Al_{0.63}Si_4$. *Chemistry of Materials* **2013,** *25* (20), 4113-4121.

52. Jung, H., Solid state NMR and pair distribution function analysis studies of Ge and Sn anodes for Li-ion batteries. *Stony Brook Theses and Dissertations Collection* **2015**.

53. Sethuraman, V. A.; Srinivasan, V.; Bower, A. F.; Guduru, P. R., In Situ Measurements of Stress-Potential Coupling in Lithiated Silicon. *Journal of The Electrochemical Society* **2010,** *157* (11).

54. Yamamura, H.; Nobuhara, K.; Nakanishi, S.; Iba, H.; Okada, S., Investigation of the irreversible reaction mechanism and the reactive trigger on SiO anode material for lithium-ion battery. *Journal of the Ceramic Society of Japan* **2011,** *119* (1395), 855-860.

For Table of Contents Only: